



HAL
open science

Ferrimagnet GdFeCo Characterization for Spin-Orbitronics: Large Field-Like and Damping-Like Torques

Héloïse Damas, Alberto Anadon, David Céspedes-Berrocal, Junior Alegre-Saenz, Jean-Loïs Bello, Aldo Arriola-Córdova, Sylvie Migot, Jaafar Ghanbaja, Olivier Copie, Michel Hehn, et al.

► **To cite this version:**

Héloïse Damas, Alberto Anadon, David Céspedes-Berrocal, Junior Alegre-Saenz, Jean-Loïs Bello, et al.. Ferrimagnet GdFeCo Characterization for Spin-Orbitronics: Large Field-Like and Damping-Like Torques. *physica status solidi (RRL) - Rapid Research Letters*, inPress, 16 (6), pp.2200035. 10.1002/pssr.202200035 . hal-03858944

HAL Id: hal-03858944

<https://hal.science/hal-03858944>

Submitted on 18 Nov 2022

HAL is a multi-disciplinary open access archive for the deposit and dissemination of scientific research documents, whether they are published or not. The documents may come from teaching and research institutions in France or abroad, or from public or private research centers.

L'archive ouverte pluridisciplinaire **HAL**, est destinée au dépôt et à la diffusion de documents scientifiques de niveau recherche, publiés ou non, émanant des établissements d'enseignement et de recherche français ou étrangers, des laboratoires publics ou privés.



Distributed under a Creative Commons Attribution 4.0 International License

Ferrimagnet GdFeCo Characterization for Spin-Orbitronics: Large Field-Like and Damping-Like Torques

Héloïse Damas,* Alberto Anadon, David Céspedes-Berrocal, Junior Alegre-Saenz, Jean-Loïs Bello, Aldo Arriola-Córdova, Sylvie Migot, Jaafar Ghanbaja, Olivier Copie, Michel Hehn, Vincent Cros, Sébastien Petit-Watelot,* and Juan-Carlos Rojas-Sánchez*

Spintronics is showing promising results in the search for new materials and effects to reduce energy consumption in information technology. Among these materials, ferrimagnets are of special interest because they can produce large spin currents that trigger the magnetization dynamics of adjacent layers or even their own magnetization. Herein, a study of the generation of spin current by GdFeCo in a GdFeCo/Cu/NiFe trilayer where the FeCo sublattice magnetization is dominant at room temperature is presented. Magnetic properties such as the saturation magnetization are deduced from magnetometry measurements while damping constant is estimated from spin-torque ferromagnetic resonance (ST-FMR). It is shown that the overall damping-like (DL) and field-like (FL) effective fields as well as the associated spin Hall angles can be reliably obtained by performing the dependence of ST-FMR by an added dc current. The sum of the spin Hall angles for both the spin Hall effect (SHE) and the spin anomalous Hall effect (SAHE) symmetries is: $\theta_{DL}^{SAHE} + \theta_{DL}^{SHE} = -0.15 \pm 0.05$ and $\theta_{FL}^{SAHE} + \theta_{FL}^{SHE} = 0.026 \pm 0.005$. From the symmetry of ST-FMR signals, it is found that θ_{DL}^{SHE} is positive and dominated by the negative θ_{DL}^{SAHE} . The present study paves the way for tuning the different symmetries in spin conversion in highly efficient ferrimagnetic systems.

1. Introduction


In the past years, ferrimagnets have attracted growing interest for their potential utility in spintronic devices.^[1] In particular, GdFeCo ferrimagnetic alloy is extensively studied as it exhibits a wide diversity of phenomena arising from the specific properties of rare earth-transition metal (RE-TM) ferrimagnets. Furthermore, the two antiferromagnetically coupled sublattices have a different response to external stimuli and the spin-orbit coupling (SOC) of the Gd 5*d* state allows the interplay between charge, spin, and orbital transport. The different relaxation times of these two coupled sublattices are thought to be responsible for the all-optical helicity-independent switching (AO-HIS) in GdFeCo demonstrated for almost a decade.^[2,3] AO-HIS has also been recently observed in TbCo.^[4] Nowadays, GdFeCo is used to perform the AO-HIS of Co/Pt^[5-7] or CoNi/Pt^[8] ferromagnetic multilayers. Moreover, it is possible to tune

the Dzyaloshinskii–Moriya interaction in thin GdFeCo ferrimagnetic alloys,^[9] a relevant property for skyrmions formation. It has been shown that GdFeCo ferrimagnet also hosts large self-induced spin-orbit torque, or self-torque,^[10,11] with recent theoretical advances.^[12,13] Ferro- and ferrimagnetic materials are the source of spin currents with different symmetries^[10,12] coming from the spin anomalous Hall effect (SAHE)^[14-16] and the spin Hall effect (SHE).^[17] In the SAHE, the spin polarization of the spin current J_s^{SAHE} is parallel to the magnetization, while in the SHE it is perpendicular to both the injected charge current and the produced spin current J_s^{SHE} . A giant overall spin Hall angle for SAHE- and SHE-like symmetries has been reported in a Gd-rich GdFeCo/Cu at room temperature.^[10] Sizable interconversion efficiencies have also been reported for other magnetic materials such as NiFe^[18-20] and CoFeB.^[15,21] In the present work, we study room temperature FeCo-rich GdFeCo in a //Gd₂₅Fe_{65.6}Co_{9.4}(8 nm)/Cu(4 or 6 nm)/Ni₈₁Fe₁₉(4 nm) trilayer by structural, magnetic, and spintronics characterization. We use two complementary ST-FMR techniques to reveal the signs and magnitudes of the contributions coming from the different spin current symmetries in GdFeCo, namely, the modulation of

H. Damas, A. Anadon, D. Céspedes-Berrocal, J. Alegre-Saenz, J.-L. Bello, A. Arriola-Córdova, S. Migot, J. Ghanbaja, O. Copie, M. Hehn, S. Petit-Watelot, J.-C. Rojas-Sánchez
CNRS, Institute Jean Lamour
Université de Lorraine
F-54 000 Nancy, France
E-mail: heloise.damas@univ-lorraine.fr; sebastien.petit@univ-lorraine.fr; juan-carlos.rojas-sanchez@univ-lorraine.fr

D. Céspedes-Berrocal, J. Alegre-Saenz, A. Arriola-Córdova
Facultad de Ciencias
Universidad Nacional de Ingeniería
Rímac 15 333, Peru

V. Cros
Unité Mixte de Physique
CNRS
Thales
Université Paris-Saclay
91 767 Palaiseau, France

 The ORCID identification number(s) for the author(s) of this article can be found under <https://doi.org/10.1002/pssr.202200035>.

DOI: 10.1002/pssr.202200035

the damping along with the shift of resonance field to extract the overall parameters (sum of the SHE- and SAHE-like contributions) and the symmetry of the ST-FMR signal which is sensitive only to the SHE-like parameters. We found that damping-like (DL) SAHE spin Hall angle, θ_{DL}^{SAHE} , is negative for FeCo-rich GdFeCo. In contrast, the DL SHE-like symmetry is positive.

2. Structural and Chemical Characterization

Samples were grown on thermally oxidized Si wafers using dc magnetron sputtering at room temperature with an Ar gas pressure of 3 mTorr and base pressure of 1×10^{-7} Torr. GdFeCo ($Gd_{25}Fe_{65.6}Co_{9.4}$) was codeposited using separate Gd, Co, and Fe targets. All the samples in the present study were capped with 3 nm of naturally oxidized Al. Transmission electron microscopy (TEM) investigations were carried out using a JEM-ARM 200 F Cold FEG TEM/STEM (scanning TEM). High-resolution TEM (HRTEM) micrographs were performed to study the atomic structure of the deposit layers, as shown in **Figure 1a**. The fast Fourier transformation (FFT) patterns in **Figure 1b,c** confirm that the Cu/NiFe layers are [111] textured along the growth direction, while GdFeCo is amorphous as evidenced by the diffuse

rings. Electron energy loss spectroscopy (EELS) maps were carried out systematically on the different samples and confirm the nominal composition and thickness of the different materials (**Figure 1d**). We also evidence a slight GdFeCo composition variation along the growing direction as usually observed in RE- ferrimagnets.^[10,11,22]

3. Magnetic Characterization: Magnetic Anisotropies in GdFeCo

3.1. SQUID Magnetometry

Magnetization loops were performed at room temperature on a //GdFeCo(8)/Cu(6)/NiFe(4) stack with the applied field parallel and perpendicular to the field plane. Both $M(H)$ measurements are displayed in **Figure 2a**, showing an open hysteresis loop. This confirms that the NiFe magnetization direction \hat{m}_{NiFe} lies in the plane of the sample while that of GdFeCo, \hat{m}_{GdFeCo} , is spontaneously perpendicular to the film plane as shown in the inset. We assume that the 6 nm-thick Cu layer decouples the two magnetic layers to extract their distinct saturation magnetization and saturation magnetic field. The coercive field is below 2 mT (50 mT) for NiFe (GdFeCo). For NiFe, the saturation

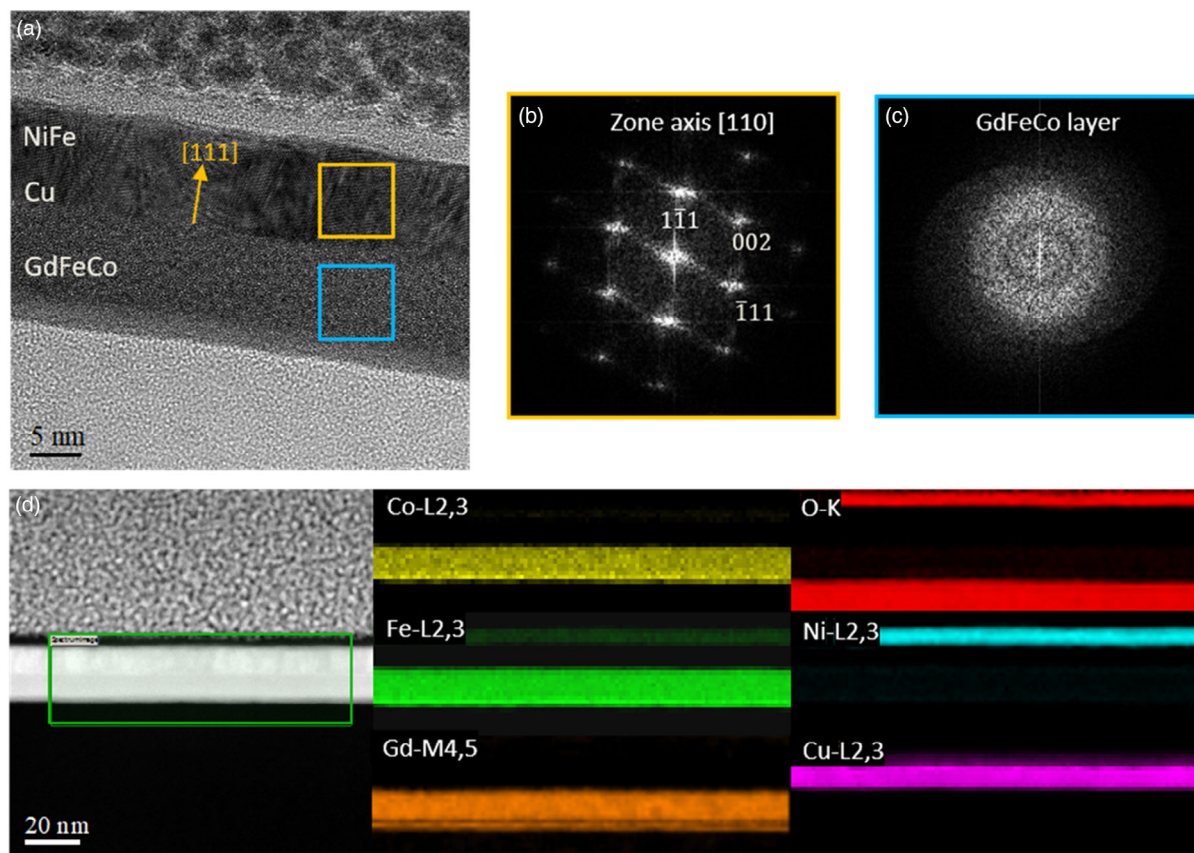


Figure 1. TEM/STEM characterization of $Gd_{25}Fe_{65.6}Co_{9.4}(8)/Cu(6)/Ni_{81}Fe_{19}(4)/AlO_x$. a) HRTEM micrograph of the deposited layers. The yellow (blue) square shows where the FFT analysis has been performed on Cu/NiFe (GdFeCo). The FFT patterns (b) and (c) indicate the [111] growth direction of textured Cu/NiFe and that GdFeCo is amorphous. d) High-angle annular dark field (HAADF)-STEM micrograph and the corresponding individual EELS elemental maps obtained from the green rectangle area in the HAADF micrograph. Co (yellow), Fe (green), Gd (orange), O (red), Ni (cyan), and Cu (pink).

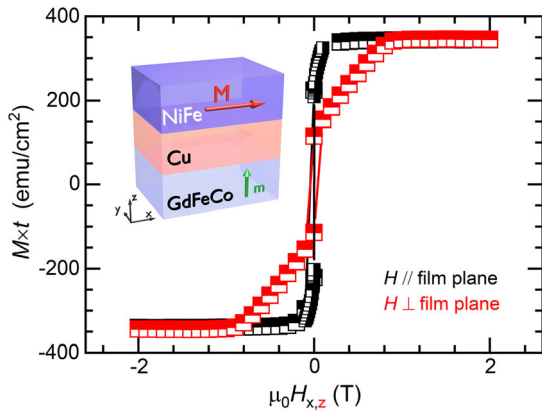


Figure 2. Bulk magnetization data using a SQUID magnetometer. a) Magnetic hysteresis loop of the $\text{Gd}_{25}\text{Fe}_{65.6}\text{Co}_{9.4}(8)/\text{Cu}(6)/\text{Ni}_{81}\text{Fe}_{19}(4)$ trilayer. Magnetization values are normalized by the surface sample. To identify the different saturation fields and effective saturation magnetization, we consider that the magnetic layers are decoupled by the 6 nm of Cu. The inset shows a schematic of the sample with the spontaneous magnetization alignment of GdFeCo (out-of-plane) and NiFe (in-plane) according to SQUID results.

magnetization M_s^{NiFe} is 625 kA m^{-1} and the saturation field $\mu_0 H_{\text{sat-z}}^{\text{NiFe}}$ to place \hat{m}_{NiFe} out of the plane of the film is 0.85 T.

In the case of GdFeCo, the saturation magnetization M_s^{GdFeCo} is 115 kA m^{-1} and the saturation field $\mu_0 H_{\text{sat-xy}}^{\text{GdFeCo}}$ to align \hat{m}_{GdFeCo} along the plane is about 0.13 T which are typical values for both NiFe and $\text{Gd}_{25}\text{Fe}_{65.6}\text{Co}_{9.4}$ at room temperature.^[23–25] From the saturation field and magnetizations, we can also estimate the effective saturation magnetization for both magnetic materials; it results $M_{\text{eff}}^{\text{NiFe}} = 676 \text{ kA m}^{-1}$ and $M_{\text{eff}}^{\text{GdFeCo}} = 103 \text{ kA m}^{-1}$. The relatively low perpendicular magnetic anisotropy of GdFeCo allows its magnetization to be easily placed along the plane of the film which is useful for ST-FMR measurements. The trilayer used in the next section has a 4 nm Cu spacer and displays a lower saturation field $\mu_0 H_{\text{sat-xy}}^{\text{GdFeCo}}$ to align \hat{m}_{GdFeCo} along the plane, which is about $\approx 0.047 \text{ T}$.

3.2. ST-FMR Study

We perform ST-FMR measurements^[26–31] on a GdFeCo(8)/Cu(4)/NiFe(4) trilayer to extract properties such as the damping constant α and the Landé g -factor of the magnetic layers. From Magneto optic Kerr effect measurements, we have verified that this GdFeCo(8) is FeCo-rich at room temperature. The experimental setup is described in Figure 3a. A radiofrequency (rf) charge current, i_{rf} , is applied along the \hat{x} direction and generates an oscillating Oersted field which triggers the magnetization

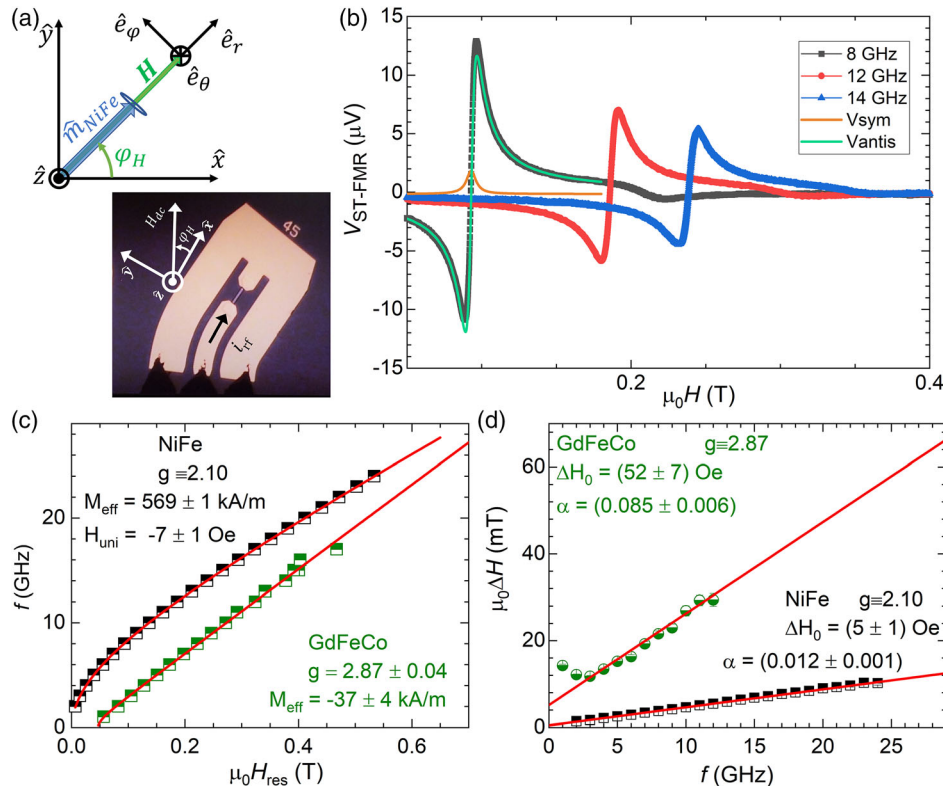


Figure 3. Determination of M_{eff} and damping using broadband ST-FMR in $\text{Gd}_{25}\text{Fe}_{65.6}\text{Co}_{9.4}(8)/\text{Cu}(4)/\text{Ni}_{81}\text{Fe}_{19}(4)$, and g -Landé factor for GdFeCo. a) Illustration of a typical ST-FMR device along with the dc magnetic field applied at φ_H to the trilayer slab which is along \hat{x} . b) Typical ST-FMR spectra at 8, 12, and 14 GHz. At higher fields, the GdFeCo resonance line is observed. The symmetrical (orange) and antisymmetrical (green) voltage contributions are shown for NiFe at 8 GHz. Broadband frequency dependence of c) H_{res} and d) linewidth ΔH are used to determine M_{eff} and α , respectively. Equation (2) is used for NiFe and GdFeCo layer in (c). For $\text{Gd}_{25}\text{Fe}_{65.6}\text{Co}_{9.4}$ (8 nm), we estimate $g = 2.87 \pm 0.04$ and $\alpha = 0.085 \pm 0.006$. Black (green) experimental data are obtained for the resonance of NiFe (GdFeCo) as depicted in (b).

precession at the resonance condition. A sweeping dc magnetic field H_{dc} is applied in the xy plane of the device, at an angle of φ_H with respect to the current line. At the resonance field H_{res} , a dc voltage V_{mix} composed of a mixing of a symmetric and antisymmetric Lorentzians of amplitude V_{sym} and V_{anti} , respectively, can be measured using a bias tee. The measured mixed voltage displayed in Figure 3b can be fitted with the following general expression

$$V_{mix} = V_{offset} + V_{sym} \frac{\Delta H^2}{\Delta H^2 + (H - H_{res})^2} + V_{anti} \frac{(H - H_{res})\Delta H}{\Delta H^2 + (H - H_{res})^2} \quad (1)$$

where we consider an additional offset V_{offset} and where ΔH is the linewidth. In Figure 3b, we observe the two resonance lines corresponding to the NiFe resonance (lower resonance field) and the GdFeCo resonance (higher resonance field). For the sake of clarity, it is only shown at 8, 12, and 14 GHz. Then, from broadband frequency dependence ST-FMR we can extract the effective saturation magnetization M_{eff} (it results negative for systems where perpendicular magnetic anisotropy dominates over shape anisotropy) and the Landé g -factor considering the following expression

$$f = \frac{\gamma}{2\pi} \sqrt{(H + H_{uni})(M_{eff} + H + H_{uni})} \quad (2)$$

where $\gamma = \frac{g\mu_B}{\hbar}$ is the gyromagnetic ratio and where H_{uni} stands for a small in-plane uniaxial magnetic anisotropy. Equation (2) applies for a thin film ferromagnetic layer with a magnetic field applied in the plane. We fix the NiFe Landé g -factor to 2.10. We determine the effective saturation magnetization of NiFe, $M_{eff}^{NiFe} = 569 \pm 1$ kA/m. The difference with previous SQUID results comes from the difference in Cu thickness which affects the NiFe anisotropy. We also evaluate a rather small $H_{uni} = -7 \pm 1$ Oe. We exploit the same Equation (2) for GdFeCo resonance condition to determine the GdFeCo Landé g -factor and its effective saturation magnetization M_{eff}^{GdFeCo} . We obtain $g = 2.87 \pm 0.04$, and $M_{eff}^{GdFeCo} = -37 \pm 4$ kA m⁻¹ (-46.5 mT). The fitted experimental data are shown in Figure 3c. Finally, from the frequency dependence of the linewidth ΔH , we calculate the Gilbert-type magnetic damping constant α

$$\Delta H = \Delta H_0 + \frac{2\pi f}{\gamma} \alpha \quad (3)$$

where ΔH_0 is the f -independent contribution due to inhomogeneity. We have fixed g -Landé factor for both NiFe and GdFeCo. The fits on the measurements are shown in Figure 3d. The damping of in-plane NiFe is estimated as $\alpha^{NiFe} = 0.012 \pm 0.001$ which is about 8 times smaller than the damping of our out-of-plane Gd₂₅Fe_{65.6}Co_{9.4} $\alpha^{GdFeCo} = 0.085 \pm 0.006$ but comparable with in-plane Gd_{12.5}Fe_{76.1}Co_{11.4}.^[32] Recently, it has been pointed out that actual or intrinsic damping in ferrimagnets is lower than that measured directly due to different spin density for each magnetic sublattice in GdFeCo and determined by domain wall mobility.^[33]

In the next section, we show how we can estimate the effective fields that drive the spin-orbit torque from Gd₂₅Fe_{65.6}Co_{9.4}(8)/Cu(4) to Ni₈₁Fe₁₉(4).

4. Damping-like and Field-like Efficiencies Determination by ST-FMR Techniques

4.1. Spin-Torque Symmetries and ST-FMR Signal

As discussed, there are two symmetries for spin current generation in magnetic materials, SAHE-like and SHE-like. When these spin currents are absorbed by another magnetic layer, they contribute to the total torque on the magnetization

$$\mathbf{\Gamma}_{tot} = \mathbf{\Gamma}_{SHE} + \mathbf{\Gamma}_{SAHE} \quad (4)$$

In the geometry of our ST-FMR measurements, the GdFeCo and NiFe magnetizations are both aligned with an angle of φ_H with respect to the \hat{x} axis. The spin polarization corresponding to the SHE-like symmetry, $\hat{\sigma}_{SHE}$, lies along the \hat{y} axis regardless of the direction of both magnetizations. The spin polarization direction related to the SAHE-like spin current, $\hat{\sigma}_{SAHE}$, lies along the direction of \hat{m}_{GdFeCo} which, in turn, is aligned with the equilibrium direction of the NiFe magnetization, \hat{m}_{NiFe} . The different contributions to the total torque can further be divided into two contributions, coming from the damping-like (h_{DL}) and the field-like (h_{FL}) effective fields

$$\frac{\mathbf{\Gamma}_{SHE}}{\gamma M_S^{NiFe}} = h_{DL}^{SHE} \hat{m}_{NiFe} \times \left(\underbrace{\hat{\sigma}_{SHE}}_{\hat{y}} \times \hat{m}_{NiFe} \right) + h_{FL}^{SHE} \hat{m}_{NiFe} \times \underbrace{\hat{\sigma}_{SHE}}_{\hat{y}} \quad (5a)$$

$$\frac{\mathbf{\Gamma}_{SAHE}}{\gamma M_S^{NiFe}} = h_{DL}^{SAHE} \hat{m}_{NiFe} \times \left(\underbrace{\hat{\sigma}_{SAHE}}_{\hat{m}_{GdFeCo}} \times \hat{m}_{NiFe} \right) + h_{FL}^{SAHE} \hat{m}_{NiFe} \times \underbrace{\hat{\sigma}_{SAHE}}_{\hat{m}_{GdFeCo}} \quad (5b)$$

The efficiency of the charge-to-spin current conversion is described by the spin Hall angles $\theta_{DL(FL)}^{SAHE}$ and $\theta_{DL(FL)}^{SHE}$. They are related to the SAHE- and SHE-like effective fields generated by GdFeCo and acting on NiFe layer as follows^[14,15,34,35]

$$h_{DL(FL)}^{SHE} = \frac{\hbar}{2|e|} \frac{J_c^{GdFeCo}}{\mu_0 M_s^{NiFe} t_{NiFe}} \theta_{DL(FL)}^{SHE} \quad (6a)$$

$$h_{DL(FL)}^{SAHE} = \frac{\hbar}{2|e|} \frac{(\hat{m}_{GdFeCo} \times J_c^{GdFeCo}) \cdot \hat{z}}{\mu_0 M_s^{NiFe} t_{NiFe}} \theta_{DL(FL)}^{SAHE} \quad (6b)$$

with $(\hat{m}_{GdFeCo} \times J_c^{GdFeCo}) \cdot \hat{z} = \sin(\varphi_H) J_c^{GdFeCo}$ in our geometry, as depicted in Figure 3a.

We show in the following subsections that ST-FMR techniques can be useful tools to further study the sign and quantification of the different contributions. Indeed, the analytical expression for the longitudinal voltage obtained by ST-FMR measurements reads^[15,27,36,37]

$$V_{dc} = -\frac{\Delta R_{AMR}^{NiFe}}{2} \sin(2\varphi_H) I_{rf} (\chi'_{\varphi\theta} \Delta h_\theta + \chi'_{\varphi\varphi} \Delta h_\varphi) \quad (7)$$

where ΔR_{AMR}^{NiFe} is the anisotropic magnetoresistance amplitude, $\chi'_{\varphi\theta}$ and $\chi'_{\varphi\varphi}$ are, respectively, the real part of the $\varphi\theta$ and the $\varphi\varphi$ components of the susceptibility matrix of NiFe, and Δh_θ and Δh_φ are, respectively, the polar and azimuthal component of the exciting field Δh (whose expression is discussed in the next subsection). We can see that only the transverse components of the excitation fields contribute to the ST-FMR voltage. We will discuss the different contributions to the total torque: 1) first considering the symmetries of Equation (7) and 2) adding a dc current which will modify the susceptibility components.

We highlight here that all the equations and signs that our model describes have been verified by considering the results obtained in a //Pt(5)/NiFe(4) reference system, namely, in this system, $\theta_{DL} = \theta_{DL}^{SHE} > 0$ and $\theta_{FL} = \theta_{FL}^{SHE} > 0$ (with a negative Oersted field).

4.2. Symmetry of the ST-FMR Signal

The NiFe magnetization resonance is triggered by the rf current-induced Oersted field, and the spin torques described in Equation (5a,b). We gather the different contributions under the general term of the exciting field, Δh . Here, the delta means that the excitation is weak. The dynamics around the equilibrium position, which takes place in the $(\hat{e}_\theta, \hat{e}_\varphi)$ plane in spherical coordinates, is only sensitive to the polar and azimuthal components of the exciting field Δh_θ and Δh_φ . As $\hat{\sigma}_{SAHE}$ lies along the NiFe magnetization equilibrium position $\hat{m}_{NiFe} = \hat{e}_r$, the associated SAHE effective fields do not contribute to the magnetization dynamics. On the contrary, the effective fields associated to the SHE-like symmetry contribute to the dynamics because $\hat{\sigma}_{SHE} \parallel \hat{y}$ and $\Delta h_\theta = h_{DL}^{SHE} \cos(\varphi_H)$ and $\Delta h_\varphi = \cos(\varphi_H)(h_{Oe} - h_{FL}^{SHE})$.^[36,37] As at the resonance $\chi'_{\varphi\varphi}$ is an antisymmetric function of the applied magnetic field and $\chi'_{\varphi\theta}$ is a symmetric function, we can express the symmetrical voltage V_{sym} amplitude and the anti-symmetrical amplitude V_{anti} introduced in Equation (1) by replacing the suitable expressions in Equation (7)

$$V_{sym} = -\sin(\varphi_H) \frac{1}{4\mu_0} \frac{I_{rf} \Delta R_{AMR}^{NiFe}}{(2H + M_{eff}^{NiFe})} \frac{2\pi f}{\gamma} \frac{h_{DL}^{SHE}}{\Delta H} \quad (8)$$

$$V_{anti} = -\sin(\varphi_H) \frac{1}{4\mu_0} \frac{I_{rf} \Delta R_{AMR}^{NiFe}}{(2H + M_{eff}^{NiFe})} \frac{2\pi f}{\gamma} \left[1 + \frac{M_{eff}}{H_{res}} \right]^{\frac{1}{2}} \frac{h_{Oe} - h_{FL}^{SHE}}{\Delta H} \quad (9)$$

V_{sym} (V_{anti}) only depends on $h_{DL}^{SHE}(h_{Oe} - h_{FL}^{SHE})$, but the extraction of the effective fields using Equation (8) and (9) is not trivial because the rf current has to be evaluated. Nevertheless, we can discuss the signs of the SHE effective fields. As depicted in Figure 3b, V_{sym} is positive which means that $h_{DL}^{SHE} > 0$. V_{anti} is negative, and thus $h_{FL}^{SHE} > 0$ assuming that the Oersted field is lower than the FL effective field.

4.3. Adding a dc Bias in ST-FMR: Damping Modulation and Shift of H_{res}

When adding a dc bias to the previous ST-FMR measurement, a constant torque is applied on the oscillating magnetization which results in a change in the expression of its dynamical susceptibility matrix. This change induces a modulation of the linewidth and a shift in the resonant field, which can be both probed by the ST-FMR technique with an added dc bias. We emphasize that the direction of the spin polarizations does not directly influence the linewidth changes or the resonant field shift: it is the projection of the spin polarization $\hat{\sigma}_{SHE, SAHE}$ along the equilibrium position of NiFe magnetization. The modulation of the linewidth and the shift of the resonance field are thus sensitive to both the SHE- and SAHE-like symmetries and allow to extract overall parameters.

In the limit of low current densities where we can neglect strong heating contribution that deformed the linear behavior, we can modify the expressions developed for magnetic tunnel junctions,^[38,39] to apply it in our system.^[10,15,26] For the modulation of the NiFe linewidth, it reads

$$\frac{\partial \Delta H_{NiFe}}{\partial i_{dc}} = -\frac{f}{\gamma_{NiFe}} \frac{2}{(2H_{res}^{NiFe} + M_{eff}^{NiFe})} \frac{S_{GdFeCo}}{W t_{GdFeCo}} \times \left(\underbrace{\hat{\sigma}_{SAHE} \cdot \hat{m}_{NiFe}}_1 \frac{\partial h_{DL}^{SAHE}}{\partial J_c^{GdFeCo}} + \frac{\hat{\sigma}_{SHE} \cdot \hat{m}_{NiFe}}{\sin(\varphi_H)} \frac{\partial h_{DL}^{SHE}}{\partial J_c^{GdFeCo}} \right) \quad (10)$$

where the left-hand term in the equation is the slope of the modulation of NiFe linewidth, $\gamma_{NiFe} = \frac{e \mu_B}{\hbar}$. S_{GdFeCo} accounts for the shunting of the GdFeCo layer by the other conductive layers, i.e., the current density flowing in GdFeCo layer is $J_c^{GdFeCo} = \frac{S_{GdFeCo}}{W t_{GdFeCo}} i_{dc}$ with W being the width of the slab (10 μ m). For simplicity, Equation (10) can also be written in terms of the Hall angles using Equation (6a,b) in the following way

$$\frac{\partial \Delta H_{NiFe}}{\partial i_{dc}} = -\frac{f}{\gamma_{NiFe}} \frac{2}{(2H_{res}^{NiFe} + M_{eff}^{NiFe})} \frac{S_{GdFeCo}}{W t_{GdFeCo}} \times \frac{\hbar}{2|e|} \sin(\varphi_H) \frac{\theta_{DL}^{SAHE} + \theta_{DL}^{SHE}}{\mu_0 M_s^{NiFe} t_{NiFe}} \quad (11)$$

The slopes $\frac{\partial \Delta H_{NiFe}}{\partial i_{dc}}$ that account for the linewidth modulation at 8 GHz are displayed in Figure 4b for $\varphi_H = 135^\circ$ and $\varphi_H = -45^\circ$. The resistivities were determined independently through the dependence of the GdFeCo and Cu thicknesses for the different layers obtaining $\rho_{Cu} = 15 \mu\Omega \text{ cm}$, $\rho_{GdFeCo} = 175 \mu\Omega \text{ cm}$, and $\rho_{NiFe} = 40 \mu\Omega \text{ cm}$. It follows $S_{GdFeCo} = 0.11$. We note that the slopes obtained when $\varphi_H = 135^\circ$, for all the different frequencies measured, are opposite than the ones measured for the //Pt/NiFe reference sample (not shown). It indicates that the DL overall spin Hall angle, $\theta_{DL}^{SAHE} + \theta_{DL}^{SHE}$, is negative and opposite to the one of Pt where only the SHE is present. From the average of positive and negative dc fields, or 135° and -45° , and for 8, 12, and 14 GHz, we evaluate the overall DL efficiency $\theta_{DL}^{SAHE} + \theta_{DL}^{SHE} = -0.15 \pm 0.05$ for the FeCo-rich GdFeCo interfaced with Cu.

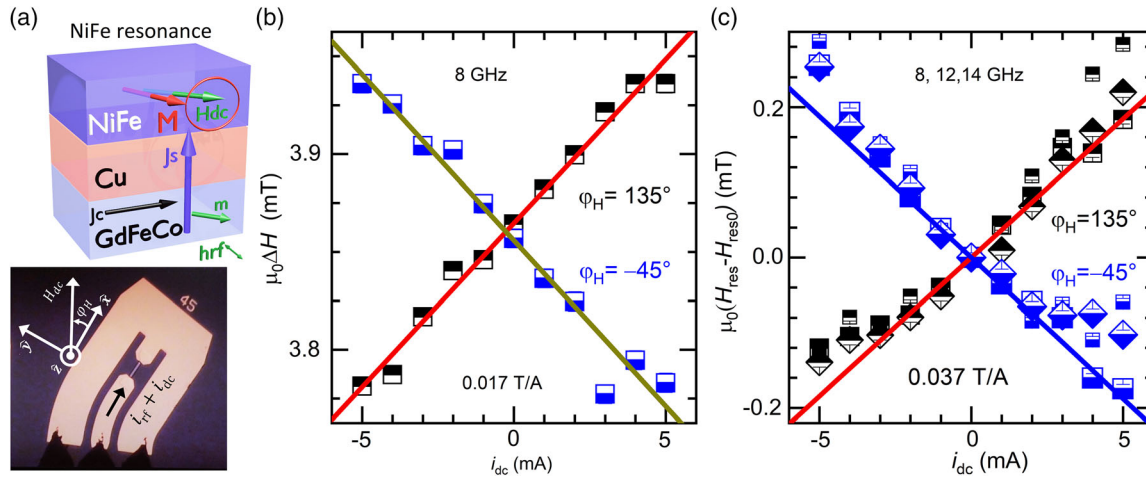


Figure 4. Damping modulation and Resonance field shift. a) Schematic of the NiFe resonance condition with additional i_{dc} current injected. b) i_{dc} dependence of the NiFe linewidth for a rf frequency of 8 GHz. c) Resonance field shift versus i_{dc} for three frequencies. Unlike the damping or linewidth modulation, we can see that the resonance field shift is frequency independent.

Furthermore, the same experiment also allows us to obtain the corresponding field-like values, h_{FL} and θ_{FL} . Based on previous studies,^[38,39] we also obtain the following expression that

accounts for the linear displacement of the resonance field with an added dc current

$$\frac{\partial H_{res}^{NiFe}}{\partial i_{dc}} = \frac{S_{GdFeCo}}{W t_{GdFeCo}} \left(\underbrace{\hat{\sigma}_{SAHE} \cdot \hat{m}_{NiFe}}_1 \frac{\partial h_{FL}^{SAHE}}{\partial J_c^{GdFeCo}} + \underbrace{\hat{\sigma}_{SHE} \cdot \hat{m}_{NiFe}}_{\sin(\varphi_H)} \frac{\partial h_{FL}^{SHE}}{\partial J_c^{GdFeCo}} \right) - \underbrace{\hat{\sigma}_{SHE} \cdot \hat{m}_{NiFe}}_{\sin(\varphi_H)} \frac{\partial h_{Oe}}{\partial i_{dc}} \quad (12)$$

where h_{Oe} is the Oersted field which lies along the $-\hat{y}$ direction in the geometry of our system. Its amplitude can be approximated with $h_{Oe} = -\frac{1}{2}(j_c^{GdFeCo} t_{GdFeCo} + j_c^{Cu} t_{Cu})$. Equation (12) reads in terms of the FL Hall angles (Equation (6a,b))

sizable overall FL value would indicate that even though GdFeCo is not in contact with NiFe, a significant FL contribution can still be detected. The origin of the FL effect in the trilayer is not clear at this stage.

$$\frac{\partial H_{res}^{NiFe}}{\partial i_{dc}} = \sin(\varphi_H) \left[\frac{S_{GdFeCo}}{W t_{GdFeCo}} \left(\frac{\hbar}{2|e|} \frac{\theta_{FL}^{SAHE} + \theta_{FL}^{SHE}}{\mu_0 M_s^{NiFe} t_{NiFe}} \right) - \frac{\partial h_{Oe}}{\partial i_{dc}} \right] \quad (13)$$

The slope obtained from the shift of the resonance field versus i_{dc} is displayed in Figure 4c for different frequencies. The parabolic pattern at high applied current may come from Joule heating. The fit on the data only considers the low current points. We observe that the slope is frequency-independent in agreement with Equation (13). Moreover, the slope has the same sign as the one in the //Pt/NiFe reference system. That implies that if there is any FL contribution on the GdFeCo/Cu/NiFe system studied here it has the same sign as for the //Pt/NiFe. The slope is evaluated as $\frac{\partial H_{res}^{NiFe}}{\partial i_{dc}} = 0.037 \text{ T/A}$. The Oersted field is approximated as $\frac{\partial h_{Oe}}{\partial i_{dc}} = -0.0476 \text{ T/A}$. Finally, considering Equation (13), the overall FL efficiency is assessed as $\theta_{FL}^{SAHE} + \theta_{FL}^{SHE} = 0.026 \pm 0.005$. This value has the same sign and is comparable to the one measured in NiFe/Pt.^[37,40] We have independently measured a control //Cu/NiFe sample without a sizable effect. We can therefore exclude the Cu/NiFe interface as the origin behind the FL measured in GdFeCo/Cu/NiFe. The

5. Discussion and Conclusions

The overall efficiencies for FeCo-rich GdFeCo/Cu/NiFe are evaluated $\theta_{DL}^{SAHE} + \theta_{DL}^{SHE} = -0.15 \pm 0.05$ and $\theta_{FL}^{SAHE} + \theta_{FL}^{SHE} = 0.026 \pm 0.005$. For sake of comparison, the SAHE efficiency of a ferromagnet such as CoFeB is $\theta_{SAHE}^{CoFeB} = -0.14$,^[15] and the SHE efficiency of Pt heavy metal is $\theta_{SHE}^{Pt} = 0.056 - 0.076$.^[29,41,42] Seki *et al.* show in FePt that DL $\theta_{SAHE+SHE}^{FePt} = 0.25$ from the linewidth modulation.^[43]

The damping-like SAHE contribution dominates over the SHE one: $|\theta_{DL}^{SAHE}| > |\theta_{DL}^{SHE}|$ with a negative SAHE contribution for FeCo-rich GdFeCo and a positive SHE contribution. We also show that the field-like SHE contribution is positive. However, we cannot estimate the individual value of each contribution. We perform the same experiments at 15 K where our ferrimagnet is Gd-rich and its magnetization aligns in-plane with a field above 0.4 T. From the sign of the symmetric contribution, we confirm that SHE remains positive when crossing the magnetic compensation temperature. This is consistent with the fact that the SHE does not depend on the GdFeCo magnetic properties. In contrast, we cannot conclude of any θ_{DL}^{SAHE} sign change because

the modulation of linewidth experiments at 15 K is hidden by others effect that are out of the scope of this study. However, the large variation in absolute value between these results and the one previously reported, for a Gd-rich GdFeCo at room temperature, $|\theta_{DL}^{SAHE} + \theta_{DL}^{SHE}| = 0.80 \pm 0.05$,^[10] suggest that the sign of θ_{DL}^{SAHE} changes between FeCo- and Gd-rich samples. If so, the opposite DL-SAHE sign for FeCo-rich GdFeCo might indicate that the SAHE spin polarization comes always from the same magnetic sublattice. Despite that, further studies could be carried out to confirm that.

GdFeCo can thus generate efficient spin currents and the different symmetries allow this material to be used in a wide variety of devices for spintronics. For instance, the SHE spin current can generate self-torque^[10] and can be used for the electrical switching of the magnetization, as shown in epitaxial FePt^[44] or CoTb.^[45] Also, the total spin current (SAHE + SHE) can be used to induce a torque on another magnetic layer or for the manipulation of skyrmions.

In summary, we have studied FeCo-rich GdFeCo/Cu/NiFe heterostructure at room temperature. First, structural and chemical analyses were performed by HRTEM and EELS. Then, the magnetic properties and the relevant spin-orbitronics parameters were determined by combining magnetometry, spin-torque ferromagnetic resonance, and additional dc current dependence. The overall damping- and field-like efficiencies, which include the SHE- and the SAHE-like symmetries, are $\theta_{DL}^{SAHE} + \theta_{DL}^{SHE} = -0.15 \pm 0.05$ and $\theta_{FL}^{SAHE} + \theta_{FL}^{SHE} = 0.026 \pm 0.005$ at room temperature. We show that SAHE dominates over SHE contribution on the DL torque. Furthermore, this study shows that the SHE contribution does not change sign when crossing the magnetic compensation temperature, while SAHE may change sign depending on the dominant sublattice of the ferrimagnet. All this underlines the importance of GdFeCo, and RE- ferrimagnets in general, as promising materials in spintronics for the exploitation of their strong spin-orbit torque.

Acknowledgements

The authors acknowledge A. Fert for fruitful discussions. This work was supported by Agence Nationale de la Recherche (France) under contract ANR-19-CE24-0016-01 (TOPTRONIC), ANR-20-CE24-0023 (CONTRABASS), and ANR-17-CE24-0025 (TOPSKY), by the French PIA project “Lorraine Université d’Excellence”, reference ANR-15IDEX-04-LUE, and by the « SONOMA » project co-funded by FEDER-FSE Lorraine et Massif des Vosges 2014-2020, a European Union Program. D.C.B. and J.A.S. also thank 2019 and 2021 Master-LUE program internship. Devices in the present study were patterned at MiNaLor clean-room platform which was partially supported by FEDER and Grand Est Region through the RaNGE project.

Conflict of Interest

The authors declare no conflict of interest.

Data Availability Statement

The data that support the findings of this study are available from the corresponding author upon reasonable request.

Keywords

ferrimagnet GdFeCo, spin anomalous Hall effect, spin Hall effect, spin-orbit torque, spin-torque ferromagnetic resonance

Received: January 31, 2022

Revised: March 10, 2022

Published online:

- [1] S. K. Kim, G. S. D. Beach, K.-J. Lee, T. Ono, T. Rasing, H. Yang, *Nat. Mater.* **2022**, 21, 24.
- [2] T. A. Ostler, J. Barker, R. F. L. Evans, R. W. Chantrell, U. Atxitia, O. Chubykalo-Fesenko, S. El Moussaoui, L. Le Guyader, E. Mengotti, L. J. Heyderman, F. Nolting, A. Tsukamoto, A. Itoh, D. Afanasiev, B. A. Ivanov, A. M. Kalashnikova, K. Vahaplar, J. Mentink, A. Kirilyuk, T. Rasing, A. V. Kimel, *Nat. Commun.* **2012**, 3, 666.
- [3] L. Le Guyader, S. El Moussaoui, M. Buzzi, R. V. Chopdekar, L. J. Heyderman, A. Tsukamoto, A. Itoh, A. Kirilyuk, T. Rasing, A. V. Kimel, F. Nolting, *Appl. Phys. Lett.* **2012**, 101, 022410.
- [4] L. Avilés-Félix, A. Olivier, G. Li, C. S. Davies, L. Álvaro-Gómez, M. Rubio-Roy, S. Auffret, A. Kirilyuk, A. V. Kimel, T. Rasing, L. D. Buda-Prejbeanu, R. C. Sousa, B. Dieny, I. L. Prejbeanu, *Sci. Reports* **2020**, 101, 1.
- [5] J. Gorchon, C. H. Lambert, Y. Yang, A. Pattabi, R. B. Wilson, S. Salahuddin, J. Bokor, *Appl. Phys. Lett.* **2017**, 111, 042401.
- [6] S. Iihama, Y. Xu, M. Deb, G. Malinowski, M. Hehn, J. Gorchon, E. E. Fullerton, S. Mangin, *Adv. Mater.* **2018**, 30, 1804004.
- [7] Q. Remy, J. Igarashi, S. Iihama, G. Malinowski, M. Hehn, J. Gorchon, J. Hohlfield, S. Fukami, H. Ohno, S. Mangin, *Adv. Sci.* **2020**, 7, 2001996.
- [8] J. Igarashi, Q. Remy, S. Iihama, G. Malinowski, M. Hehn, J. Gorchon, J. Hohlfield, S. Fukami, H. Ohno, S. Mangin, *Nano Lett.* **2020**, 20, 8654.
- [9] Y. Quessab, J. W. Xu, C. T. Ma, W. Zhou, G. A. Riley, J. M. Shaw, H. T. Nembach, S. J. Poon, A. D. Kent, *Sci. Rep.* **2020**, 10, 1.
- [10] D. Céspedes-Berrocá, H. Damas, S. Petit-Watetot, D. Maccariello, P. Tang, A. Arriola-Córdova, P. Vallobrá, Y. Xu, J. Bello, E. Martín, S. Migot, J. Ghanbaja, S. Zhang, M. Hehn, S. Mangin, C. Panagopoulos, V. Cros, A. Fert, J. Rojas-Sánchez, *Adv. Mater.* **2021**, 33, 2007047.
- [11] S. Krishnia, E. Haltz, L. Berges, L. Aballe, M. Foerster, L. Bocher, R. Weil, A. Thiaville, J. Sampaio, A. Mougin, *Phys. Rev. Appl.* **2021**, 16, 1.
- [12] K. Kim, K. Lee, *Phys. Rev. Lett.* **2020**, 125, 207205.
- [13] H. Ochoa, R. Zarzuela, Y. Tserkovnyak, *J. Magn. Magn. Mater.* **2021**, 538, 168262.
- [14] T. Taniguchi, J. Grollier, *Phys. Rev. Appl.* **2015**, 044001, 1.
- [15] S. Iihama, T. Taniguchi, K. Yakushiji, A. Fukushima, Y. Shiota, S. Tsunegi, R. Hiramatsu, S. Yuasa, Y. Suzuki, H. Kubota, *Nat. Electron.* **2018**, 1, 120.
- [16] C. Safranski, E. A. Montoya, I. N. Krivorotov, *Nat. Nanotechnol.* **2018**, 141, 27.
- [17] V. P. Amin, P. M. Haney, M. D. Stiles, *J. Appl. Phys.* **2020**, 128, 151101.
- [18] K. S. Das, W. Y. Schoemaker, B. J. Van Wees, I. J. Vera-Marun, *Phys. Rev. B* **2017**, 96, 1.
- [19] W. Wang, T. Wang, V. P. Amin, Y. Wang, A. Radhakrishnan, A. Davidson, S. R. Allen, T. J. Silva, H. Ohldag, D. Balzar, B. L. Zink, P. M. Haney, J. Q. Xiao, D. G. Cahill, V. O. Lorenz, X. Fan, *Nat. Nanotechnol.* **2019**, 14, 819.
- [20] M. Haidar, A. A. Awad, M. Dvornik, R. Khymyn, A. Houshang, J. Åkerman, *Nat. Commun.* **2019**, 10, 1.

- [21] C. Safranski, J. Z. Sun, J. W. Xu, A. D. Kent, *Phys. Rev. Lett.* **2020**, *124*, 197204.
- [22] D. Kim, M. Haruta, H. Ko, G. Go, H. Park, T. Nishimura, D. Kim, T. Okuno, Y. Hirata, Y. Futakawa, H. Yoshikawa, W. Ham, S. Kim, H. Kurata, A. Tsukamoto, Y. Shiota, T. Moriyama, S. Choe, K. Lee, T. Ono, *Nat. Mater.* **2019**, *18*, 685.
- [23] M. Ding, S. J. Poon, *J. Magn. Magn. Mater.* **2013**, *339*, 51.
- [24] K. Wang, Y. Tang, K. Zhang, Y. Wang, J. Liu, *Mater. Sci. Eng. B* **2021**, *263*, 114848.
- [25] S. Nayak, S. S. Das, B. B. Singh, T. R. Charlton, C. J. Kinane, S. Bedanta, *RSC Adv.* **2020**, *10*, 34266.
- [26] L. Liu, T. Moriyama, D. C. Ralph, R. A. Buhrman, *Phys. Rev. Lett.* **2011**, *106*, 1.
- [27] D. Fang, H. Kurebayashi, J. Wunderlich, K. Výborný, L. P. Zárbo, R. P. Campion, A. Casiraghi, B. L. Gallagher, T. Jungwirth, A. J. Ferguson, *Nat. Nanotechnol.* **2011**, *6*, 413.
- [28] K. Kondou, H. Sukegawa, S. Mitani, K. Tsukagoshi, S. Kasai, *Appl. Phys. Express* **2012**, *5*, 1.
- [29] C. Guillemard, S. Petit-Watelot, S. Andrieu, J.-C. Rojas-Sánchez, *Appl. Phys. Lett.* **2018**, *113*, 262404.
- [30] E. Liu, T. Fache, D. Cespedes-Berrocal, Z. Zhang, S. Petit-Watelot, S. Mangin, F. Xu, J.-C. Rojas-Sánchez, *Phys. Rev. Appl.* **2019**, *12*, 044074.
- [31] J. Xu, A. D. Kent, *Phys. Rev. Appl.* **2020**, *10*, 1.
- [32] L. Bainsla, A. Kumar, A. A. Awad, C. Wang, M. Zahedinejad, N. Behera, H. Fulara, R. Khymyn, A. Houshang, J. Weissenrieder, J. Åkerman, *Adv. Funct. Mater.* **2021**.
- [33] D. Kim, T. Okuno, S. K. Kim, S. Oh, T. Nishimura, Y. Hirata, Y. Futakawa, H. Yoshikawa, A. Tsukamoto, Y. Tserkovnyak, Y. Shiota, T. Moriyama, K. Kim, K. Lee, T. Ono, *Phys. Rev. Lett.* **2019**, *122*, 127203.
- [34] A. V. Khvalkovskiy, V. Cros, D. Apalkov, V. Nikitin, M. Krounbi, K. A. Zvezdin, A. Anane, J. Grollier, A. Fert, *Phys. Rev. B* **2013**, *87*, 20402.
- [35] C. F. Pai, Y. Ou, L. H. Vilela-Leão, D. C. Ralph, R. A. Buhrman, *Phys. Rev. B Condens. Matter Mater. Phys.* **2015**, *92*.
- [36] T. Fache, *Iridium-Based Synthetic Ferrimagnets For Spintronics*, Université de Lorraine, Lorraine, France **2020**.
- [37] H. Damas, Spin-Orbit Torques by Second Harmonic and Spin-Torque Ferromagnetic Resonance Revisited, **2022**, Unpublished.
- [38] S. Petit, C. Baraduc, C. Thirion, U. Ebels, Y. Liu, M. Li, P. Wang, B. Dieny, *Phys. Rev. Lett.* **2007**, *98*, 3.
- [39] S. Petit, N. De Mestier, C. Baraduc, C. Thirion, Y. Liu, M. Li, P. Wang, B. Dieny, *Phys. Rev. B - Condens. Matter Mater. Phys.* **2008**, *78*, 184420.
- [40] T. Nan, S. Emori, C. T. Boone, X. Wang, T. M. Oxholm, J. G. Jones, B. M. Howe, G. J. Brown, N. X. Sun, *Phys. Rev. B* **2015**, *91*, 214416.
- [41] J. C. Rojas-Sánchez, N. Reyren, P. Laczowski, W. Savero, J. P. Attané, C. Deranlot, M. Jamet, J. M. George, L. Vila, H. Jaffrès, *Phys. Rev. Lett.* **2014**, *112*.
- [42] T. Fache, J. C. Rojas-Sanchez, L. Badie, S. Mangin, S. Petit-Watelot, *Phys. Rev. B* **2020**, *102*, 064425.
- [43] T. Seki, S. Iihama, T. Taniguchi, K. Takanashi, *Phys. Rev. B* **2019**, *100*, 144427.
- [44] K. Dong, C. Sun, L. Zhu, Y. Jiao, Y. Tao, X. Hu, R. Li, S. Zhang, Z. Guo, S. Luo, X. Yang, S. Li, L. You, *Engineering* **2022**, <https://doi.org/10.1016/j.eng.2021.09.018>.
- [45] Z. Zheng, Y. Zhang, V. Lopez-Dominguez, L. Sánchez-Tejerina, J. Shi, X. Feng, L. Chen, Z. Wang, Z. Zhang, K. Zhang, B. Hong, Y. Xu, Y. Zhang, M. Carpentieri, A. Fert, G. Finocchio, W. Zhao, P. Khalili Amiri, *Nat. Commun.* **2021**, *12*, 4555.